THE JOURNAL OF PHYSICAL CHEMISTRY C

ARTICLE

pubs.acs.org/JPCC

Water-Soluble Magnetic Nanoparticles Functionalized with Photosensitizer for Photocatalytic Application

Kyong-Hoon Choi,[†] Kang-Kyun Wang,[†] Eon Pil Shin,[†] Seung-Lim Oh,[†] Jin-Seung Jung,[‡] Hwan-Kyu Kim,[§] and Yong-Rok Kim*[,†]

[†]Department of Chemistry, Yonsei University, Seoul 120-749, Republic of Korea

[‡]Department of Chemistry, Gangneung-Wonju National University, Gangneung 210-702, Republic of Korea

[§]Department of Advanced Materials Chemistry, Korea University, Jochiwon, Chungnam 339-700, Republic of Korea

ABSTRACT: We report a novel photofunctional magnetic nanoparticle that is strategically designed and prepared by simple modification process. Photofunctionality is provided by the photosensitizer (PS) of [5,15-bis(phenyl)-10,20-bis(4-methoxycarbonylphenyl)porphyrin]platinum that generates singlet oxygen in high quantum yield. The PS molecules are covalently bonded to the surface of magnetic nanoparticles. Microstructure and magnetic and photophysical properties of the photofunctional magnetic nanoparticles are investigated by transmission electron microscopy, vibrating sample magnetometry, and time-resolved spectroscopic methods. The results show that the immobilized PS molecules retain their optical and functional properties including the high efficiency of singlet oxygen generation. Generation quantum yield (Φ_Δ) and releasing yield (η_Δ) of singlet oxygen from the prepared photofunctional magnetic nanoparticles are 0.47 and 0.42, respectively. Furthermore, the photofunctional magnetic nanoparticles have good solubility and stability in water, which are induced by the surface modification process. The photocatalytic experiment is demonstrated by utilizing the oxidation reaction of 2,4,6-trichlorophenol with the photofunctional magnetic nanoparticles.

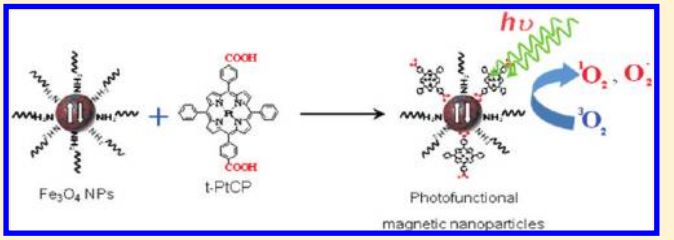

1. INTRODUCTION

In last decades, considerable attention has been attracted to the purification of wastewater and groundwater contaminated by chlorinated compounds.[1−4] Among the chlorinated organic compounds, chlorophenols are extensively used compounds for wood preservatives, pesticides, fungicides, herbicides, insecticides, and disinfectants. They also exist even in the waste of paper mills.[5] The chlorophenols are toxic, hardly biodegradable, and difficult to remove from the environment.[6,7] Therefore, the chlorophenols have become one of the major environmental pollutants and are assigned as top priority pollutants by the U.S. EPA. Because of their toxicity to human and animal lives, stringent restrictions have increasingly been imposed on the concentration of these compounds in the wastewater for safe discharge. Therefore, it is very important to find an innovative and cost-effective method for the safe and complete destruction of chlorophenols such as 2,4,6-trichlorophenol (2,4,6-TCP) and pentachlorophenol.

Several technologies of activated carbon adsorption, incineration, membrane filtration, ion exchange, electrochemical oxidation, and biological degradation have been applied for the removal of chlorophenols.[8−12] A common disadvantage of such technologies is the fact that removal efficiency decreases markedly at a trace level. In addition, those technologies have high treatment costs and possibility of secondary pollution. Photocatalytic oxidation, an advanced oxidation process, is one of the cost-effective technologies for the degradation of chlorophenols.[13−15] The governing principle of photocatalytic oxidation in this study is the formation of reactive oxygen species that are the principal oxidizing agents for organic pollutants. Reactive oxygen species attack organic pollutants in water and convert them into CO_2 and H_2O and mineral acids. However, this photocatalytic oxidation method is limited by the separation and recollection of the utilized catalysts for recycled usage. Recently, various methodologies for catalyst separation and reactivation have extensively been developed. Among the methodologies, magnetic separation provides a very convenient approach for removing and recycling the catalysts by applying external magnetic fields.[16−19] In this regard, introduction of photocatalyst into the magnetic nanoparticle with a simple reaction can be a good solution.

In this study, we report a simple surface modification process that induces the magnetic nanoparticles to be functionalized with [5,15-bis(phenyl)-10,20-bis(4-methoxycarbonylphenyl)porphyrin]platinum (t-PtCP) without the loss of photofuctionality and magnetism. Photocatalytic activity of the photofunctional magnetic nanoparticles is evaluated by the photosensitized oxidation reaction of 2,4,6-TCP in water under visible light irradiation (λ > 450 nm).

Received: September 7, 2010
Revised: January 17, 2011
Published: February 10, 2011

Scheme 1. Synthesis of t-PtCP

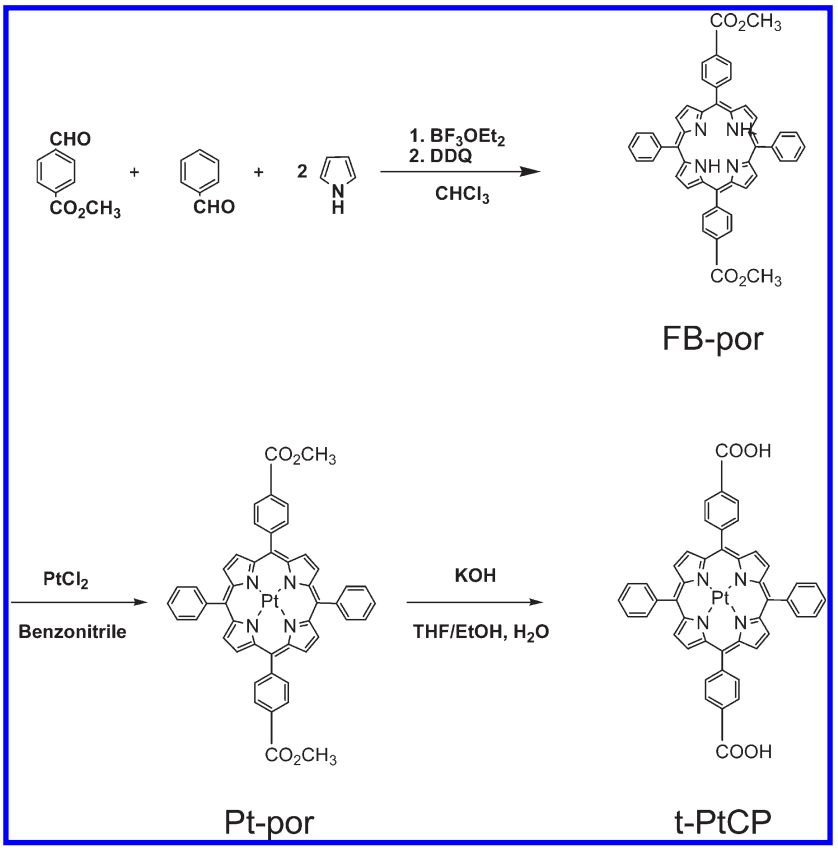

2. EXPERIMENTAL DETAILS

2.1. Preparation of the t-PtCP Molecule. Synthesis of 1,5-bis(phenyl)-10,20-bis(4-methoxycarbonylphenyl)porphyrin [FB-Por]: A mixture of methyl-4-formylbenzoate (1.5 g, 9.137 mmol), benzaldehyde (0.97 g, 9.147 mmol), and pyrrole (1.27 mL, 18.26 mmol) was condensed in chloroform (913 mL) with $BF_3 \cdot OEt_2$ (1.39 mL, 10.96 mmol) at room temperature for 1 h. Then DDQ (6.22 g, 27.41 mmol) was added. After the mixture was stirred for 1 h at room temperature, the solvent was removed under reduced pressure. The residue was then dissolved in $CHCl_3$ and passed through a short silica gel column to remove the nonporphyrinic components from the reaction mixture. This mixture was purified with a second column (silica, $CHCl_3$) to afford the compound of FB-por (86 mg, 1.4%).

^{1}H NMR ($CDCl_3$, 300 MHz) [ppm]: δ 8.87−8.81 (m, 8H, β-pyrrole), 8.46−8.43 (d, 4H, Ar−H), 8.32−8.29 (d, 4H, Ar−H), 8.29−8.23 (d, 4H, Ar−H), 7.78−7.61 (d, 4H, Ar−H), 4.12 (s, 6H, $-OCH_3$), −2.78 (s, 2H, −NH). FT-IR (KBr pellet, cm^{-1}): 1720 (ester, C═O), 3315 (amine, −NH:). FAB-MS (m/z): Calcd $C_{48}H_{34}N_4O_4$ 730.81, Found 731.0.

Synthesis of [5,15-bis(phenyl)-10,20-bis(4-methoxycarbonylphenyl)porphyrin]platinum [Pt(II)-por]: FB-por (0.5 g, 0.68 mmol) and $PtCl_2$ (0.46 g, 1.71 mmol) were suspended in anhydrous benzonitrile. The mixture was then purged with N_2 and slowly heated to 160 °C. It was then brought to reflux under N_2 until there was no free base left as revealed by TLC (24 h). The mixture was then cooled to room temperature, and the solvent was removed by vacuum distillation. The resulting product was then dried completely and purified with a column (silica, CH_2Cl_2) to afford the compound of Pt(II)-por (400 mg, 86%).

^{1}H NMR ($CDCl_3$, 300 MHz) [ppm]: 8.78−8.68 (m, 8H, β-pyrrole), 8.43−8.41 (d, 4H, Ar−H), 8.25−8.22 (d, 4H, Ar−H), 8.15−8.12 (d, 4H, Ar−H), 7.75−7.31 (d, 4H, Ar−H), 4.10 (s, 6H, $-OCH_3$). FT-IR (KBr pellet, cm^{-1}): 1720 (ester, C═O). FAB-MS (m/z): Calcd $C_{48}H_{32}N_4O_4Pt$ 923.87, Found 924.0

Synthesis of [5,15-bisphenyl-10,20-bis(4-carboxyphenyl)-porphyrin]platinum [Pt(II)-por-COOH]: Pt(II)-Por (0.6 g, 0.65 mmol) and KOH (0.36 g, 6.49 mmol) were dissolved in THF−EtOH−H_2O (in a volume/volume ratio of 1:1:0.1, 50 mL), and the solution was refluxed for 12 h. The mixture was cooled to room temperature and neutralized with HCl. It was then extracted with CH_2Cl_2. The organic phase was washed with sodium bicarbonate aqueous solution and dried with sodium sulfate. Removal of the solvent yielded Pt(II)-por-COOH (500 mg, 85.9%).

^{1}H NMR (DMSO, 300 MHz) [ppm]: 8.74 (s, 8H, β-pyrrole), 8.37−8.34 (d, 4H, Ar−H), 8.30−8.27 (d, 4H, Ar−H), 8.17−8.15 (d, 4H, Ar−H), 7.82−7.80 (d, 4H, Ar−H). FT-IR (KBr pellet, cm^{-1}): 1690 (carboxylic acid, C═O), 2400−3400 (carboxylic acid, −COOH). FAB-MS (m/z): Calcd $C_{46}H_{28}N_4O_4Pt$ 895.82, Found 896.0.

The prepared t-PtCP molecule (Scheme 1) is easy to be bonded to the surface of magnetic nanoparticles due to the two terminal groups of carboxylic acid which lead to the covalent bonding. Also, the t-PtCP molecule has a high singlet oxygen quantum yield of 0.65 ± 0.05 in solution. This value of singlet oxygen quantum yield is higher than the other photosensitizers such as hematoporphyrin (0.51)[20] and protoporphyrin (0.63).[21] Therefore,

dx.doi.org/10.1021/jp1085137 |J. Phys. Chem. C 2011, 115, 3212–3219

Scheme 2. Fabrication Procedure of the Photofunctional Magnetic Nanoparticles

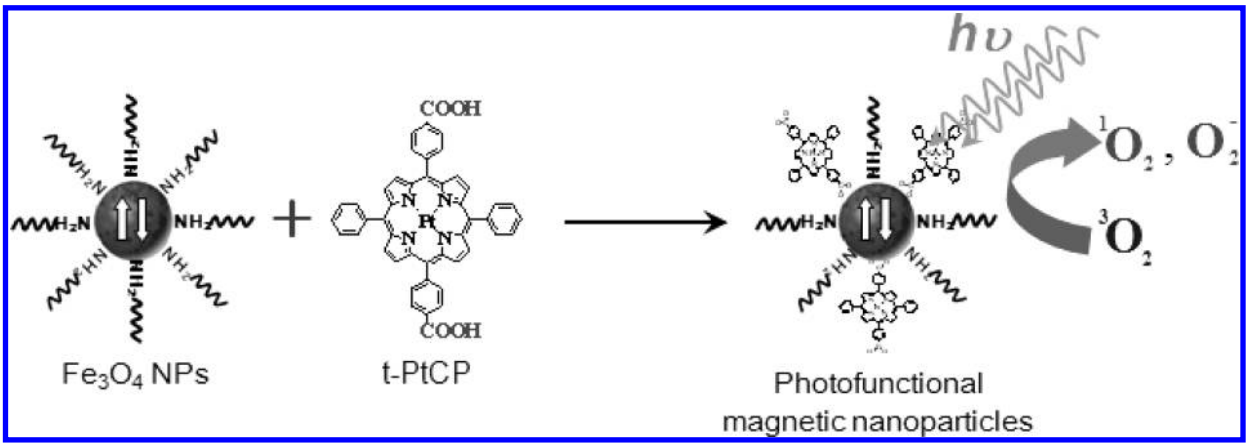

based on these factors, the t-PtCP molecule is utilized as a photosensitizer in this study.

2.2. Preparation of the Photofunctional Magnetic Nanoparticles. Magnetite (Fe_3O_4) nanoparticles covered with oleylamine were prepared by applying a similar method as that in the previous report.[22] $Fe(acac)_3$, 1,2-hexadecanediol, oleylamine, and phenyl ether were mixed and magnetically stirred under a flow of nitrogen. The mixture solution was heated to 200 °C for 30 min and, under a blanket of nitrogen, refluxed under the same temperature for another 30 min. The dark-brown mixture solution was cooled to room temperature. Under ambient conditions, ethanol was added to the mixture. The black compound was precipitated and separated with centrifugation. Then it was redispersed in hexane.

Photofunctionality on the magnetic nanoparticles was provided by a wet chemical process with t-PtCP as follows. The precipitated magnetic nanoparticles (1.5 mg) were mixed with the solution of t-PtCP/THF (1.8×10^{-2} mM). The mixture solution was agitated for 24 h at room temperature. After the reaction was completed, the product was then washed with THF solution several times. The concentration of t-PtCP molecules bound to the surfaces of the magnetic nanoparicles was estimated by using UV−visible absorption spectroscopy. The relative absorption OD at a wavelength of 510 nm (corresponding to the Q-band of t-PtCP) between a stock solution of t-PtCP (1.8×10^{-2} mM) and the remaining solution obtained after removing the magnetic aggregation in the magnetic nanoparticle solution resulted in the reacted concentration of t-PtCP molecules with the nanoparticles. Therefore, from the result, it was estimated that $\sim 6.6 \times 10^{-8}$ mol (equivalent to 3.98×10^{16} molecules) of t-PtCP was immobilized onto the surface of 1 mg of magnetic nanoparticles. Assuming the density of the magnetic nanoparticles to be 5.4 g/cm^3, 1 mg of magnetic nanoparticles contains 2.85×10^{15} particles.[23] Consequently, there are approximately 14 t-PtCP molecules that are immobilized on the surface of each magnetic nanoparticle.

2.3. Characterization of the Photofunctional Magnetic Nanoparticles. Transmission electron microscopy (TEM, JEOL JEM-2100F) was applied to determine the size and shape of the photofunctional magnetic nanoparticles. Crystallographic characteristics and nanostructure of the composite nanoparticles were investigated with an X-ray diffractometer (XRD, PANalytical, Pert Pro MPD) working on Cu Kα radiation. A vibrating sample magnetometry (VSM, Lakeshore 7300) was utilized to measure the magnetization versus magnetic field loop at room temperature up to $H = 10$ kOe. Infrared spectra were obtained using a FT-IR spectrometer (Perkin-Elmer 100). For IR measurements, samples were prepared in an agate mortar and then prepared in the form of pressed wafers (ca. 1% sample in KBr). Absorption and emission spectra were obtained from an UV−vis spectrophotometer (Hitachi, U-2800) and spectrofluorometer (Hitachi, F-4500), respectively.

2.4. Direct Detection of Singlet Oxygen Generated by the Photofunctional Magnetic Nanoparticles. Quantum yield of singlet oxygen ($\Phi_\Delta(^1O_2)$) and its lifetime were measured by detecting a near-IR phosphorescence emission peak at 1270 nm.[24] The phosphorescence signal was collected with a germanium photodiode (EG&G, Judson) at the perpendicular angle to the excitation beam through cutoff (<1000 nm, CVI) and interference filters (1270 nm, spectrogon). A Nd:YAG pumped OPO laser (B. M. Industries, OP901-355, 5 ns fwhm pulse) was utilized as an excitation source. The signal was acquired by a 500 MHz digital oscilloscope and transferred to a computer for data analysis.

2.5. Indirect Detection of the Singlet Oxygen. Degradation of 1,3-diphenylisobenzofuran (DPBF) of a singlet oxygen quencher was applied to determine the release of singlet oxygen into the solution.[25] An aliquot of 3.5 mL of THF solution containing the photofunctional magnetic nanoparticles or 5,10,15,20-tetraphenyl-21*H*,23*H*-porphine (H_2TPP) (1.42×10^{-5} M) that is used as a standard reference was introduced to a 1 cm quartz cell under dark conditions with DPBF (1.0×10^{-5} M). The experiments were carried out by irradiating the samples with laser light (λ = 510 nm, 7.5 mW/cm^2) with the nanosecond-pulsed Nd:YAG pumped OPO laser. Photodegradation of DPBF was monitored by recording the OD of the absorption peak at 435 nm. The OD change was measured as a function of irradiation time. Singlet oxygen releasing efficiency (η_Δ) of the photofunctional magnetic nanoparticles was determined by the following equation, using H_2TPP solution in THF as a standard.[26]

$$\eta_{\Delta\text{particle}} = \varphi_{H_2TTP}\frac{t_{H_2TTP}}{t_{\text{particle}}}$$

where t_{H_2TPP} is a time constant of the first-order exponential decay fitted to the decrease in the absorption peak of DPBF during the photocatalytic degradation reaction with free H_2TPP/THF solution, t_{particle} is the same time constant as above for the absorption decrease of DPBF in the presence of the photofunctional magnetic

dx.doi.org/10.1021/jp1085137 |J. Phys. Chem. C 2011, 115, 3212–3219

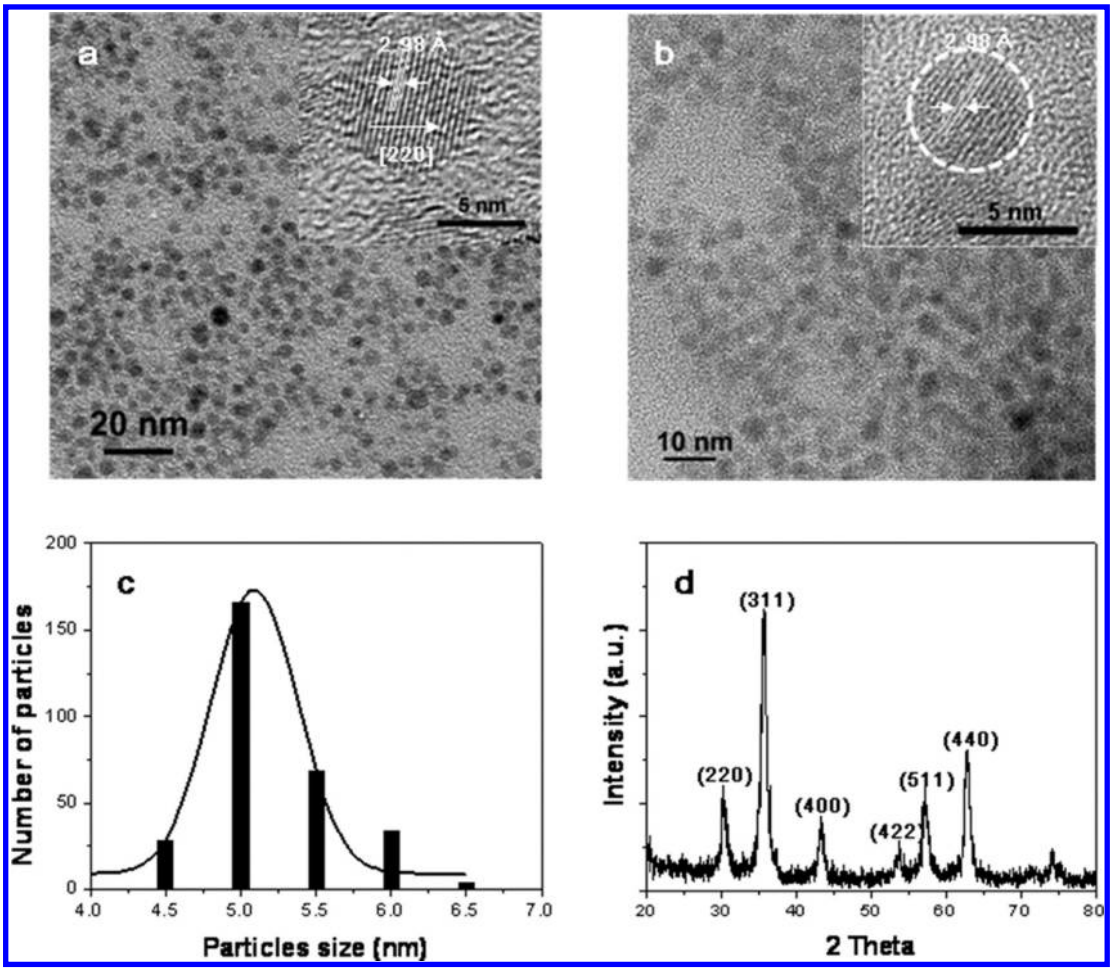

Figure 1. TEM micrographs of (a) the pure magnetite nanoparticles and (b) the photofunctional magnetic nanoparticles. Corresponding high-resolution TEM images of the individual nanoparticles are shown in the insets. (c) Histogram for the particle size distribution of the pure magnetite nanoparticles. (d) XRD pattern of the pure magnetite nanoparticles.

nanoparticles in THF solution, and φ_{H_2TPP} is the singlet oxygen quantum yield of free H_2TPP in THF solution which is given as 0.62.[27]

2.6. Photocatalytic Reaction with the Photofunctional Magnetic Nanoparticles. A photocatalytic degradation experiment of 2,4,6-TCP was carried out under visible light irradiation in the aqueous solution where the photofunctional magnetic nanoparticles were suspended. The suspension solution was prepared by adding 10 mg of the photofunctional magnetic nanoparticles into 20 mL of aqueous 2,4,6-TCP solution with an initial concentration of 7.5×10^{-5} M. Before irradiation of visible light, the mixture solution was magnetically stirred under dark conditions for 1 h to achieve an equilibrium state. Air was bubbled into the suspension solution for 30 min before visible irradiation. An Xe lamp (150 W, Abet Technologies, U.S.) was used as the irradiation source. The distance between the lamp and the solution was 50 cm, and the light radiation intensity at the sample was measured to be 28.5 mW/cm^2. A 450 nm glass cutoff filter was used to remove ultraviolet light, so that only the Q bands were irradiated. This UV cutoff also prevents direct photodegradation of 2,4,6-TCP from UV light irradiation. At every 20 min of irradiation, absorption spectra of the samples were observed with a UV−vis spectrophotometer.

3. RESULTS AND DISCUSSION

As illustrated in Scheme 2, the photofunctional magnetic nanoparticles were prepared by the surface modification of magnetic nanoparticles with a photosensitizer of t-PtCP. The carboxyl terminal group of t-PtCP is chemically bonded to Fe ions on the surface of magnetic nanoparticles with the surface complexation structure.[28,29]

Morphologies and crystal structures of the pure magnetite nanoparticles and the photofunctional magnetic nanoparticles were investigated by using TEM and XRD. The pure magnetite nanoparticles and the photofunctional magnetic nanoparticles both have spherical shapes, and they are well dispersed on the TEM grids as shown in Figure 1a and b. It is noted that, after the surface modification, there is no significant changes observed in the particle size and morphology. Figure 1c shows the size distribution histogram of the magnetite nanoparticles, which is estimated from 300 particles in different regions of the TEM micrograph. It presents the size uniformity with an average particle size of 5.2 ± 0.4 nm. The high-resolution TEM images (insets of Figure 1a and b) show that both nanoparticles have a single crystalline nature. The distance between two neighboring planes is approximately 2.98 Å, which is consistent with that of the (220) planes of an inverse spinel-structured magnetite nanoparticle.[30]

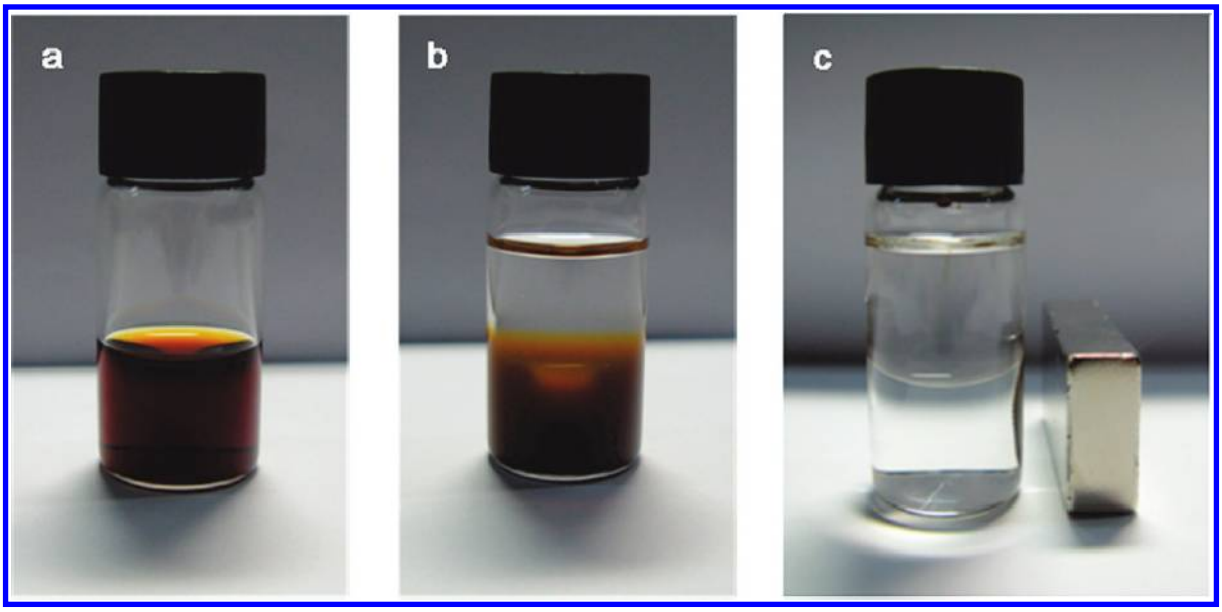

Figure 2. Solubility of magnetic nanoparticles before and after the surface modification. (a) As-synthesized nanoparticles in hexane. (b) Nanoparticles modified with t-PtCP in water. The upper layer presents hexane. (c) t-PtCP-modified nanoparticles in the presence of an external magnetic field.

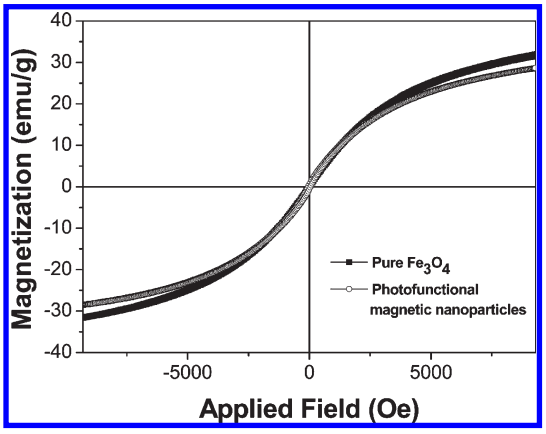

Figure 3. Room-temperature magnetic hysteresis loops of the pure magnetites and the photofunctional magnetic nanoparticles.

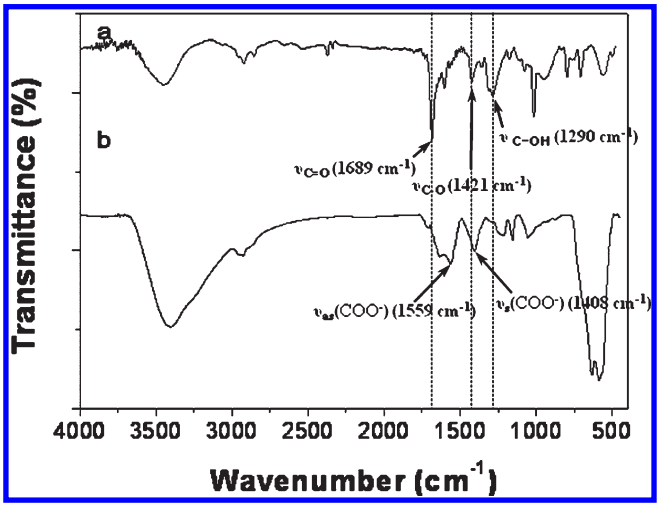

Figure 4. FT-IR spectra of (a) the pure t-PtCP and (b) the photofunctional magnetic nanoparticles.

The powder XRD pattern of the magnetite nanoparticles provides more detailed structural information as shown in Figure 1d. The strong Bragg reflection peaks (2θ = 30.0, 35.6, 43.3, 53.7, 57.0, anf 62.8°) are marked by their Miller indices ((220), (311), (400), (422), (511), and (440)) from standard Fe_3O_4 powder diffraction data (JCPDS, card 19-0629), which are the characteristic peaks of the magnetite crystal of cubic inverse spinel structure.[31] The average particle diameter of 5.0 nm estimated from Scherrer's equation is in a good agreement with the value that is determined by statistical analysis of the TEM image, which implies that each individual particle is a single crystal. Scherrer's equation is expressed as the following[32]

$$D = \frac{0.9\lambda}{B \cos \theta_B}$$

where λ is the wavelength used, B is the full width at half-maximum (fwhm) measured in radians on the 2θ scale, and θ_B is the Bragg angle for the measured hkl peak.

Figure 2 displays solubility of the magnetic nanoparticles before and after the surface-modified reaction with t-PtCP. The pure magnetite nanoparticles before the modification reaction are well dispersed in hexane (Figure 2a) due to the oleylamine groups attached on the particle surface. On the other hand, the surface-modified photofunctional magnetic nanoparticles only disperse in water as shown in Figure 2b where the phase separation appears between the upper and lower mediums of hexane and water, respectively. Water dispersity of the photofuctional nanoparticles suggests that the oleylamines on the nanoparticle are mostly replaced by t-PtCP. As shown in Figure 2c, the photofunctional magnetic nanoparticles are collected with the magnet at the outside surface of the cuvette. As the external magnet is removed, the collected particles are redispersed into water with a mild shaking.

Magnetic properties of the pure magnetite nanoparticles and the photofunctional magnetic nanoparticles were measured by

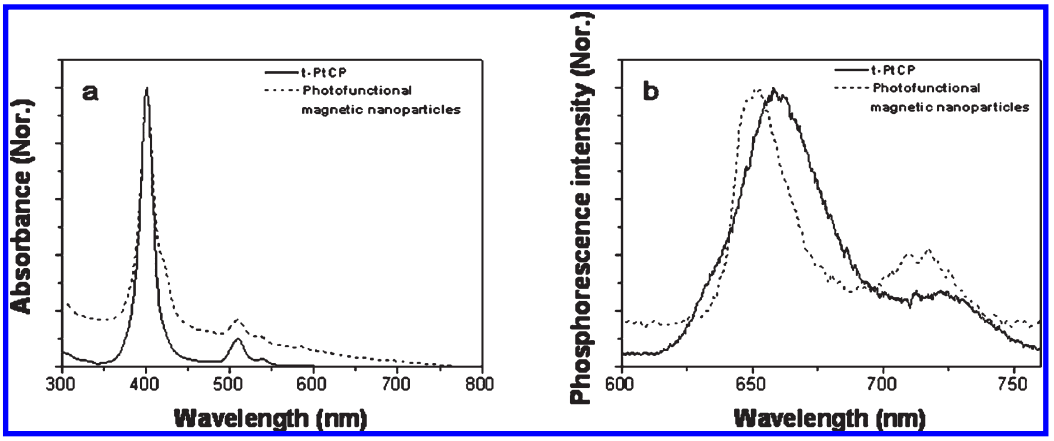

Figure 5. (a) Absorption and (b) emission spectra of the pure t-PtCP and the photofunctional magnetic nanoparticles in THF. The excitation wavelength is 510 nm for the emission spectra.

using a VSM at room temperature (Figure 3). The magnetization curves exhibit no hysteresis and no remnant magnetization even at the highest magnetic field, which implies superparamagnetic property of the nanoparticles. The pure magnetite nanoparticles show the high saturation magnetization value of 32.2 emu/g, whereas the high saturation value of the surface-modified photofunctional magnetic nanoparticles is 28.5 emu/g. The difference in the saturation values is attributed to the diamagnetic contribution of the t-PtCP molecules that are chemically bonded to the nanoparticle surface.

To confirm the bonding between the carboxyl group of the t-PtCP and the Fe ion of the Fe_3O_4 nanoparticle, FT-IR spectra of the t-PtCP and the photofunctional magnetic nanoparticles were comparatively studied (Figure 4). As reported in the previous study,[33] the IR spectrum of the pure t-PtCP presents the absorption peaks at 1689, 1421, and 1290 cm^{-1}, corresponding to the stretching modes of the free carbonyl double bond ($\upsilon_{C=O}$), the carbon−oxygen single bond (υ_{C-O}), and the O−H deformation (υ_{C-OH}), respectively. These characteristic absorption peaks suggest that the pure t-PtCP has the protonated carboxyl groups (COOH) as expected. After the chemical bonding occurs between the carboxyl group and the Fe ion, the IR bands for the protonated carboxyl group substantially disappear and the new bands appear at 1559 and 1408 cm^{-1}. These new bands are ascribed to the asymmetric (υ_{as} = 1559 cm^{-1}) and the symmetric (υ_s = 1408 cm^{-1}) stretching modes of the carboxylate group, based on the similar observation reported by Dravid et al.[34] They suggest that the IR bands at 1556 and 1410 cm^{-1} correspond to the asymmetric (υ_{as}) and the symmetric (υ_s) stretching modes of the carboxylate in their oleic acid system that has the coordination bonding between the carboxylate and the cobalt ion on the surface of the cobalt nanoparticle. In particular, in this photofunctional magnetic nanoparticle, the disappearance of $\upsilon_{C=O}$ (1689 cm^{-1}) in Figure 4b indicates that the carboxylate group is bounded to the surface of the Fe_3O_4 nanoparticle symmetrically through its two oxygen atoms.

Figure 5a shows that the absorption spectrum of the photofunctional magnetic nanoparticles has the same characteristics as that of the pure t-PtCP in THF. The peak at 400 nm is the Soret band of t-PtCP, and the Q bands are located at 510 and 538 nm. At the excitation wavelength of 408 nm, the pure t-PtCP produces two strong emission peaks located at 660 and 725 nm, and the photofunctional magnetic nanoparticles provide the slightly blue-shifted peaks at 651 and 715 nm. The blue-shifted emission peaks are attributed to the strong bonding between t-PtCP and the magnetic nanoparticle.

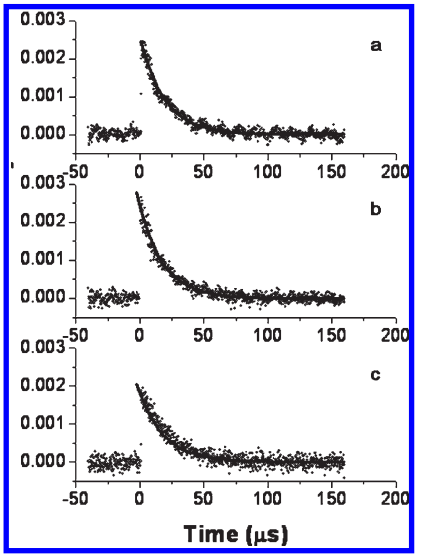

Figure 6. Phosphorescence decay induced by relaxation of the singlet oxygen from (a) H_2TPP molecules of the reference, (b) the pure t-PtCP molecules, and (c) the photofunctional magnetic nanoparticles. Phosphorescence signals are detected at 1270 nm in THF solution and fitted with a single exponential function (solid line).

Singlet oxygen generation from the photofunctional magnetic nanoparticles is confirmed with direct detection of the phosphorescence that comes from the photoexcited t-PtCPs bonded to the nanoparticles. Time-resolved singlet oxygen phosphorescence signals are presented in Figure 6. All the singlet oxygen lifetimes from H_2TPP, the pure t-PtCP, and the bounded t-PtCP in THF solutions are ~20 μs, which is in a good agreement with the value reported in the literature.[35] Singlet oxygen quantum yields (Φ_Δ) of the samples are determined by comparing the phosphorescence intensities at 1270 nm for the samples and the reference of H_2TPP in THF solution.[36] The singlet oxygen quantum yield of the photofunctional magnetic nanoparticles is estimated to be 0.47 ± 0.03, while that of the pure t-PtCP is measured to be 0.65 ± 0.05. The lower Φ_Δ value of 0.47 as compared to 0.65 is possibly due to the bonded nature of t-PtCP

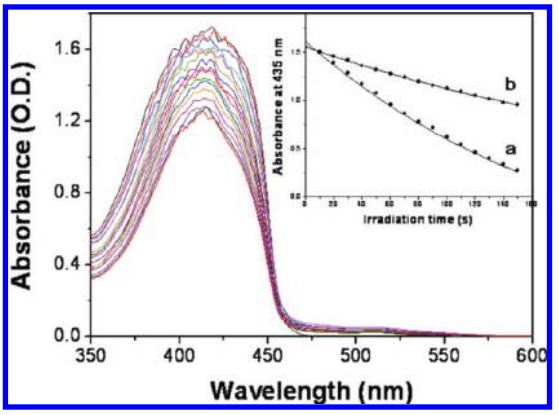

Figure 7. Irradiation time-dependent UV−vis spectra of DPBF in THF solution with the photofunctional magnetic nanoparticles excited at 510 nm of laser light. Inset represents the absorption OD of DPBF in THF at 435 nm as a function of irradiation time with (a) the pure H_2TPP and (b) the dispersed photofunctional magnetic nanoparticles.

and the magnetic nanoparticles. The t-PtCP bond nature on the surface of the particle induces closer interactions between the t-PtCP molecules than the interactions among the free molecules in the solution. Such interactions between the bonded t-PtCP molecules in high population density and the structural restriction of the bonded t-PtCP molecules are considered to cause the spectral blue-shift of the emission bands and the lesser generation of singlet oxygens. The blue-shift emission nature is previously reported for the aggregated forms of photosensitizers (PS) and the PS-bonded silica matrix.[29,37]

To estimate the release efficiency of singlet oxygen into the solution, the degradation method of DPBF is applied. As a specific singlet oxygen quencher, DPBF readily undergoes 1,4-cycloaddition reaction with singlet oxygen and forms the endo peroxides. Then it further decomposes into the irreversible product of 1,2-dibenzoylbenzene.[38] Therefore, the release amount of singlet oxygen can be monitored by observing the decrease in optical density of the DPBF absorption at 435 nm.[39] Figure 7 illustrates the temporal OD change of the DPBF absorption peak in THF with the photofunctional magnetic nanoparticles under the laser irradiation at 510 nm. Efficiency of the singlet oxygen release (η_Δ) from the photofunctional magnetic nanoparticles is measured to be 0.42 $\pm$ 0.04, which is very similar to the singlet oxygen quantum yield estimated by direct detection of the phosphorescence.

In order to check the application possibility for water purification, the photocatalytic activity of the photofunctional magnetic nanoparticles fabricated in this study is evaluated by the photocatalytic oxidation reaction of 2,4,6-TCP in an aqueous solution at pH 10 under visible light irradiation (λ > 450 nm) of the Xe lamp. Figure 8 indicates the photodegradation rate of 2,4,6-TCP as a function of irradiation time in the presence of the photofunctional magnetic nanoparticles. The spectral change indicates the decrease of 2,4,6-TCP molecules and the formation of of 2,4-dichlorobenzoquinone as the photocatalytic reaction continues since the absorption peaks at 312 and 273 nm correspond to 2,4,6-TCP and 2,4-dichlorobenzoquinone, respectively.[40] Only the photofunctional magnetic nanoaprticles efficiently degraded the 2,4,6-TCP solution under the visible light, while the light-induced decomposition of 2,4,6-TCP without the magnetic nanoparticles and the decomposition of 2,4,6-TCP induced by the photofunctional magnetic nanoparticles without the light were not observed.

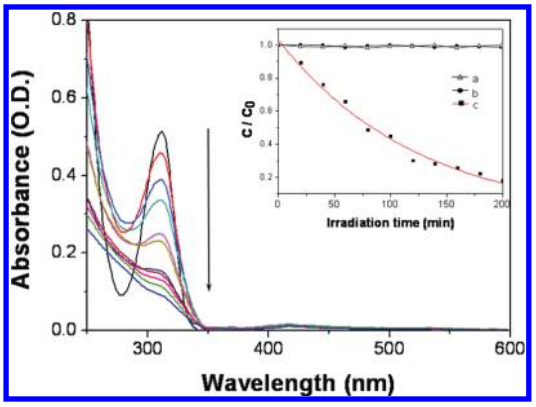

Figure 8. Absorption spectral change of 2,4,6-TCP in aqueous solution of pH 10 depending on the photocatalytic reaction time with the photofunctional magnetic nanoparticles. The visible light (>450 nm) from a Xe lamp is utilized for all measurements. The inset represents the ratio between the reaction OD (C) and the initial OD (C_o) of 2,4,6-TCP as a function of irradiation time. Inset: (a) 2,4,6-TCP only with the light, (b) 2,4,6-TCP with the photofunctional magnetic nanoparticles without the light, and (c) 2,4,6-TCP with the photofunctional magnetic nanoparticles under light conditions.

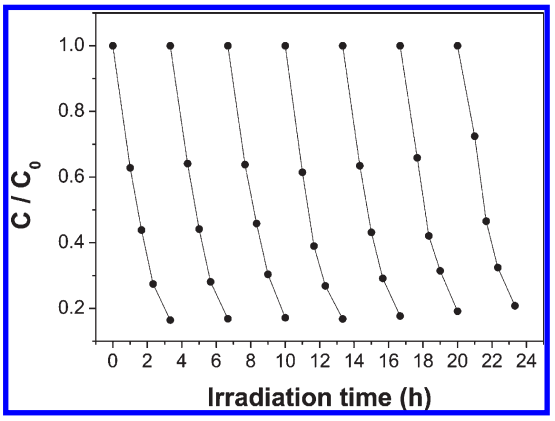

Figure 9. Recycling experiment for 2,4,6-TCP photodegradation in the presence of the photofunctional magnetic nanoparticles under visible light irradiation. C/C_o represents the ratio between the reaction OD (C) and the initial OD (C_o) of 2,4,6-TCP as a function of irradiation time.

To evaluate the stability of the photofunctional magnetic nanoparticles in the photocatalytic reaction, the recycling efficiency of the photofunctional magnetic nanoparticles was investigated. Figure 9 suggests that the photofunctional magnetic nanoparticle shows similar photocatalytic activity after five times of the recycled usage. Even after seven times of the reuse, the 2,4,6-TCP degradation efficiency with the photofunctional magnetic nanoparticles was maintained to be about 80%.

4. CONCLUSIONS

We have successfully fabricated the magnetic nanoparticles functionalized with t-PtCP using by a simple modification reaction. The t-PtCP coupled photofunctional magnetic nanoparticles have superparamagnetic property with a saturation magnetization value of 28.5 emu/g and show excellent dispersibility and stability in water. The photofunctional magnetic nanoparticles generate the singlet oxygen quantum yield of 0.47 $\pm$ 0.03 that is enough to be utilized as a recyclable photocatalyst activated by

visible light. The photocatalytic degradation experiment demonstrates that 2,4,6-TCP is effectively decomposed. Such visible activated photocatalytic property of the photofunctional magnetic nanoparticles fabricated in this study can be utilized to remove the environmental harzards in water, and, furthermore, the magnetic property of this composite particle provides the recycled usage of photocatalyst, preventing possible secondary contamination.

AUTHOR INFORMATION

Corresponding Author

*Tel. +82 2 2123 2646; fax +82 2 364 7050; e-mail yrkim@yonsei.ac.kr.

ACKNOWLEDGMENT

This work was supported by a grant of the Korea Healthcare Technology R&D Project, Ministry for Health, Welfare & Family Affairs, Republic of Korea (grant no. A085136), grant A101424 from the Korean Health Technology R&D Project, and the National Research Foundation of Korea Grant funded by the Korean Government (No. 2010-0025875). J.-S.J. is thankful for a grant from the Converging Research Center Program. through the Ministry of Education, Science and Technology (2010K001115).

REFERENCES

(1) Wong-Wah-Chung, P.; Rafqah, S.; Voyard, G.; Sarakha, M. *J. Photochem. Photobiol., A* **2007**, *191*, 201.
(2) Christoforidis, K. C.; Louloudi, M.; Milaeva, E. R.; Sanakis, Y.; Deligiannakis, Y. *Mol. Phys.* **2007**, *105*, 2185.
(3) Shen, J.; Chen, Z.; Xu, Z.; Li, X.; Xu, B.; Qi, F. *J. Hazard. Mater.* **2008**, *152*, 1325.
(4) Sharma, S.; Mukhopadhyay, M.; Murthy, Z. V. P. *Ind. Eng. Chem. Res.* **2010**, *49*, 3094.
(5) Mohamed, F. S.; Khater, W. A.; Mostafa, M. R. *Chem. Eng. J.* **2006**, *116*, 47.
(6) Keith, L. H.; Telliard, W. A. *Environ. Sci. Technol.* **1979**, *13*, 416.
(7) U.S. EPA, http://www.scorecard.org, 2002.
(8) Jain, S.; Jayaram, R. V. *Sep. Sci. Technol.* **2007**, *42*, 2019.
(9) Das, S.; Banthia, A. K.; Adhikari, B. *Chem. Eng. J.* **2008**, *138*, 215.
(10) Chan, W. C.; Fu, T. P. *J. Appl. Polym. Sci.* **1998**, *67*, 1085.
(11) Polcaro, A. M.; Palmas, S. *Ind. Eng. Chem. Res.* **1997**, *36*, 1791.
(12) Kennedy, L. J.; Lu, J.; Mohn, W. W. *Water Res.* **1992**, *26*, 1085.
(13) Ranjit, K. T.; Willner, I.; Bossmann, S.; Braun, A. *J. Phys. Chem. B* **1998**, *102*, 9397.
(14) Park, H.; Vecitis, C. D.; Choi, W.; Weres, O.; Hoffmann, M. R. *J. Phys. Chem. C* **2008**, *112*, 885.
(15) Zhou, X.; Hu, C.; Hu, X.; Peng, T.; Qu, J. *J. Phys. Chem. C* **2010**, *114*, 2746.
(16) Xu, S.; Shangguan, W.; Yuan, J.; Chen, M.; Shi, J.; Jiang, Z. *Nanotechnology* **2008**, *19*, 095606.
(17) Ye, M.; Zhang, Q.; Hu, Y.; Ge, J.; Lu, Z.; He, L.; Chen, Z.; Yin, Y. *Chem.—Eur. J.* **2010**, *16*, 6243.
(18) Zhang, L.; Wang, W.; Zhou, L.; Shang, M.; Sun, S. *Appl. Catal., B* **2009**, *90*, 458.
(19) Alvarez, P; Jaramillo, J.; Lopez-Pinero, F.; Plucinski, P. K. *Appl. Catal., B* **2010**, *100*, 338.
(20) Mathai, S.; Smith, T. A.; Ghiggino, K. P. *Photochem. Photobiol. Sci.* **2007**, *6*, 995.
(21) Rossi, L. M.; Silva, P. R.; Vono, L. L. R.; Fernandes, A. U.; Tada, D. B.; Baptista, M. S. *Langmuir* **2008**, *24*, 12534.
(22) Sun, S.; Zeng, H.; Robinson, D. B.; Raoux, S.; Rice, P. M.; Wang, S. X.; Li, G. *J. Am. Chem. Soc.* **2004**, *126*, 273.
(23) Prakash, A.; McCormick, A. V.; Zachariah, M. R. *Chem. Mater.* **2004**, *16*, 1466.
(24) Ha, J.-H.; Ko, S.; Lee, C.-H.; Lee, W.-Y.; Kim, Y.-R. *Chem. Phys. Lett.* **2001**, *349*, 271.
(25) Rossi, L. M.; Silva, P. R.; Vono, L. R.; Fernandes, A. U.; Tada, D. B.; Baptista, M. S. *Langmuir* **2008**, *24*, 12534.
(26) Tada, D. B.; Vono, L. L. R.; Duarte, E. L.; Itri, R.; Kiyohara, P. K.; Baptista, M. S.; Rossi, L. M. *Langmuir* **2007**, *23*, 8194.
(27) Schmidt, R.; Afshari, E. *J. Phys. Chem.* **1990**, *94*, 4377.
(28) Duckworth, O. W.; Martin, S. T. *Geochim. Cosmochim. Acta* **2001**, *65*, 4289.
(29) Turro, N. J.; Lakshminarasimhan, P. H.; Jockusch, S.; O'Brien, S. P.; Grancharov, S. G.; Redl, F. X. *Nano Lett.* **2002**, *2*, 325.
(30) Guo, S.; Li, D.; Zhang, L.; Li, J.; Wang, E. *Biomaterials* **2009**, *30*, 1881.
(31) Chin, S. F.; Iyer, S.; Raston, C. L. *Cryst. Growth Des.* **2009**, *9*, 2685.
(32) Galceran, M.; Pujol, M. C.; Zaldo, C.; Diaz, F.; Aguilo, M. *J. Phys. Chem. C* **2009**, *113*, 15497.
(33) Trivedi, P.; Vasudevan, D. *Environ. Sci. Technol.* **2007**, *41*, 3135.
(34) Wu, N.; Fu, L.; Su, M.; Aslam, M.; Wong, K. C.; Dravid, V. P. *Nano Lett.* **2004**, *4*, 383.
(35) Hurst, J. R.; McDonald, J. D.; Schuster, G. B. *J. Am. Chem. Soc.* **1982**, *104*, 2067.
(36) Fernandez, D. A.; Awruch, J.; Dicello, L. E. *Photochem. Photobiol.* **1996**, *63*, 784.
(37) Zenkevich, E.; Sagun, E.; Knyukshto, V.; Shulga, A.; Mironov, A.; Efremova, O.; Bonnett, R.; Songca, S. P. *J. Photochem. Photobiol., B* **1996**, *33*, 171.
(38) Fujii, M.; Usui, M.; Hayashi, S.; Gross, E.; Kovalev, D.; Künzner, N.; Diener, J.; Timoshenko, V. Y. *J. Appl. Phys.* **2004**, *95*, 3689.
(39) Wilson, T. *J. Am. Chem. Soc.* **1966**, *88*, 2898.
(40) Ozoemena, K.; Kuznetsova, N.; Nyokong, T. *J. Mol. Catal. A: Chem.* **2001**, *176*, 29.